RSC Advances

PAPER

View Article Online
View Journal | View Issue

Cite this: *RSC Adv.*, 2020, **10**, 30035

Alkaline earth metal ion coordination increases the radical scavenging efficiency of kaempferol†

Ling-Ling Qian, [a] Yao Lu, [a] Yi Xu,[a] Zhi-Yin Yang,[a] Jing Yang,[a] Yi-Ming Zhou, [a] Rui-Min Han, *[a] Jian-Ping Zhang [a] and Leif H. Skibsted [b]

Flavonoids are used as natural additives and antioxidants in foods, and after coordination to metal ions, as drug candidates, depending on the flavonoid structure. The rate of radical scavenging of the ubiquitous plant flavonoid kaempferol (3,5,7,4′-tetrahydroxyflavone, Kaem) was found to be significantly enhanced by coordination of Mg(II), Ca(II), Sr(II), and Ba(II) ions, whereas the radical scavenging rate of apigenin (5,7,4′-trihydroxyflavone, Api) was almost unaffected by alkaline earth metal (AEM) ions, as studied for short-lived β-carotene radical cations (β-Car$^{\bullet+}$) formed by laser flash photolysis in chloroform/ethanol (7 : 3) and for the semi-stable 2,2-diphenyl-1-picrylhydrazyl radical, DPPH$^{\bullet}$, in ethanol at 25 °C. A 1 : 1 Mg(II)–Kaem complex was found to be in equilibrium with a 1 : 2 Mg(II)–Kaem$_2$ complex, while for Ca(II), Sr(II) and Ba(II), only 1 : 2 AEM(II)–Kaem complexes were detected, where all complexes showed 3-hydroxyl and 4-carbonyl coordination and stability constants of higher than 10^9 L^2 mol^{-2}. The 1 : 2 Ca(II)–Kaem$_2$ complex had the highest second order rate constant for both β-Car$^{\bullet+}$ (5×10^8 L mol^{-1} s^{-1}) and DPPH$^{\bullet}$ radical (3×10^5 L mol^{-1} s^{-1}) scavenging, which can be attributed to the optimal combination of the stronger electron withdrawing capability of the (n − 1)d orbital in the heavier AEM ions and their spatially asymmetrical structures in 1 : 2 AEM–Kaem complexes with metal ion coordination of the least steric hindrance of two perpendicular flavone backbones as ligands in the Ca(II) complex, as shown by density functional theory calculations.

Received 11th April 2020
Accepted 8th July 2020

DOI: 10.1039/d0ra03249b

rsc.li/rsc-advances

Introduction

Flavonoids are among the most investigated phytochemicals due to their high abundance and structural diversity.[1] These compounds are supplied to animals and humans supplied by fruit and vegetable intake, and are associated with well-documented benefits including, anticancer, anti-inflammation, antiatherosclerotic and antioxidant properties.[2–4] The complexation of flavonoids with metal ions has been reported to significantly enhance the antioxidant activities of most of these complexes,[5–17] while for some other combinations of metal ions and flavonoids, their antioxidant activities are unchanged or even decrease.[18–22] The binding of metal ions with flavonoids and the type of metal–flavonoid complexes formed depend on solvent, pH, concentration and the nature of both the metal ions and flavonoids, which complicates the understanding of the molecular mechanism behind the effect that the metal ions have on the activities of the flavonoids.[5,6,18,19]

A remarkable increase in the radical scavenging efficiency of flavonoids by the coordination of the transition metal ions Zn(II) and Cu(II) has been demonstrated and quantitatively assigned to specific species in equilibrium in solution in our recent studies.[5,6] For both Zn(II) and Cu(II), 1 : 1 metal–flavonoid complexes were found to have a higher radical scavenging ability than 1 : 2 complexes as a result of electron withdrawal from the phenolic group of the flavonoid by metal ions.[5,6] For 1 : 2 metal complexes with two flavonoid ligands in a symmetrical structure, the electron withdrawal by transition metal ions from the ligands is balanced, and the radical scavenging activity decreases compared to that of the asymmetric 1 : 1 complexes.[5,18] In contrast, the effect that the binding of the ions of main group elements to flavonoids has on the radical scavenging activity of flavonoids and on the structure–activity is less clear.[23]

In the present study, we extend the investigation of the binding of metal ions to flavonoids and systematically explore the interactions of alkaline earth metal (AEM) ions with flavonoids and the effect on the radical scavenging efficiency of binding of AEMs to flavonoids. Ca, Sr and Ba have recently been found to mimic transition metals, showing unusual structures and reactivities.[24–26] Mg and Ca are ubiquitous and essential to living organisms, playing vital biological roles.[27,28] Sr also plays an important role in aquatic life and has found some use in medicine for improving bone strength,[29] whereas Ba is toxic to living organisms. Both Sr and Ba are included in the present

[a]*Department of Chemistry, Renmin University of China, Beijing, China, 100872. E-mail: rmhan@ruc.edu.cn; Fax: +86-10-6251-6444; Tel: +86-10-6251-6604*

[b]*Department of Food Science, University of Copenhagen, Rolighedsvej 30, DK-1958 Frederiksberg C, Denmark*

† Electronic supplementary information (ESI) available. See DOI: 10.1039/d0ra03249b

study in order to systematically elucidate the effect that AEM ions have on the radical scavenging activities of flavonoids. Kaem (3,5,7,4′-tetrahydroxyflavone) and Api (5,7,4′-trihydroxyflavone apigenin, with a 3-hydroxyl group less than kaempferol, Scheme 1), were compared for their chelation of AEM ions and for the effect of AEM ion binding on their radical scavenging efficiencies. The finding of the 1 : 2 Ca(II)–$Kaem_2$ complex as the most efficient radical scavenger should be of more general interest for the use of flavonoids as additives and antioxidants in food systems with high calcium content, such as dairy products.

Experimental

Chemicals

Kaempferol (Kaem, >98%) and apigenin (Api, >98%) from Huike Plant Exploitation Inc (Shaanxi, China), magnesium acetate $Mg(CH_3COO)_2$ (>98%) and calcium acetate $Ca(CH_3COO)_2 \cdot H_2O$ (>99%) from Titan Scientific (Shanghai, China), strontium acetate $Sr(CH_3COO)_2 \cdot 1/2H_2O$ (>99%) and barium acetate $Ba(CH_3COO)_2$ (>99%) from Shandong Xiya Chemical Co. Ltd., and 1,1-diphenyl-2-picrylhydrazyl radical (DPPH$^{\bullet}$) from ZhongShengRuiTai Technology Inc (>97%, Beijing, China) were used as received. All-*trans*-β-carotene (β-Car, >93%), ferrocene (>98%) and $NaClO_4$ (>98%) from Sigma-Aldrich (St. Louis, MO, USA) and spectrophotometric grade ethanol (99.9%, Fine Chemical Industry Research Institute, Tianjin, China) were used as received. Chloroform (>99.0%, Beijing Chemical Works, Beijing, China) was purified before use by passing it through an alumina column (AR, Tianjin Fuchen Chemical Plant, Tianjin, China).

Reaction of alkaline earth metals ions with Kaem and Api

All UV-vis absorption spectra were measured on a Cary60 spectrophotometer (Varian, Inc., Palo Alto, CA, USA) using 1.0 cm quartz cells in a thermostated room at 25 °C. The absorption spectra were obtained by two methods: (i) adding increasing amounts of AEM(II) ions to 20 μM Kaem or Api, (ii) mixing solutions of Kaem or Api and AEM(II) ions with invariable total molar concentrations but varying molar ratios from 19 : 1 to 1 : 19 for Mg(II) or Ca(II), and from 9 : 1 to 1 : 9 for Sr(II) or Ba(II) ions.

Infrared (IR) spectra and mass spectra (MS)

IR spectra were obtained on a Bruker Tensor 27 FT-IR spectrometer (Karlsruhe, Germany). Solid samples of AEM(II)–kaempferol/apigenin complexes for IR tableting were prepared from a solution of Kaem/Api and AEM(II) salts in ratios of 1 : 10 by evaporation of ethanol under a nitrogen gas flow.

MS were obtained on a Thermo Scientific™ Q Exactive™ HF (Waltham, MA, USA) spectrometer operated in positive ion mode. Samples of AEM(II)–kaempferol complexes were prepared by filtering solutions of Kaem and AEM(II) salts after mixing them through a nylon membrane with 220 nm sieve pores. The samples were analyzed by direct infusion electrospray ionization (ESI) by means of a syringe pump (Thermo UltiMate 3000, Waltham, MA, USA) at a flow rate of 5 μL min^{-1} at a capillary temperature of 320 °C and spray voltage of 3.50 kV.

Determination of oxidation potentials

Cyclic voltammetry (CV) was performed on a three-electrode CHI 760D electrochemical analyzer (ChenHua Instruments Inc., Shanghai, China) both in ethanol and in ethanol : chloroform = 7 : 3. The working electrode was a glassy carbon piece (diameter = 4 mm), the reference electrode was a silver wire, and the auxiliary electrode was a platinum wire. 0.10 M $NaClO_4$ was used as a supporting electrolyte. 50 μM ferrocene was used as an internal standard, and CVs were obtained in the potential range of −0.5 to 0.9 V at a scan rate of 0.05 V s^{-1}.

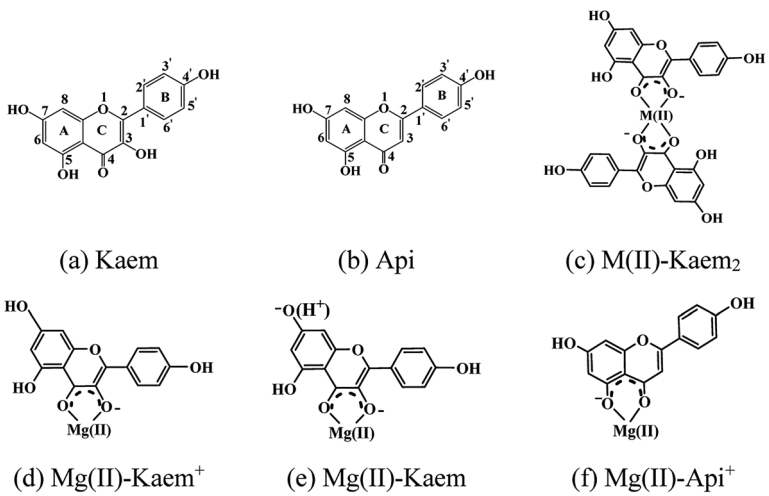

Scheme 1 Molecular structures of (a) kaempferol, (b) apigenin, (c) a 1 : 2 M(II)–$Kaem_2$ complex, M = Mg, Ca, Sr, Ba, (d) a 1 : 1 cationic Mg(II)–$Kaem^+$ complex, and (e) a 1 : 1 neutral Mg(II)–Kaem complex without a 7-phenolic proton, as the most acidic group identified from DFT calculations, (f) 1 : 1 cationic Mg(II)–Api^+ complex.

β-Carotene radical cation and DPPH˙ scavenging

The laser flash photolysis apparatus for the study of the kinetics of β-Car$^{\cdot+}$ scavenging has been previously described in detail.[30,31] The laser pulses at 532 nm (4 mJ per pulse, 7 ns, and 10 Hz) for the bleaching assay were supplied by a Nd^{3+}:YAG laser (Quanta-Ray PRO-230, Spectra Physics Lasers, Inc., Mountain View, CA, USA). 940 and 510 nm probe lights were provided by a laser-driven white light source (LDLS-EQ-99 LAMP MODULE, Energetiq Technology, Inc., Woburn, MA). The absorbance was detected using a photodiode (model S3071, Hamamatsu Photonics, Hamamatsu, Japan). The optical path length of the cuvette was 1 cm and all measurements were carried out at 25 °C. Ethanol/chloroform (7/3, v/v) was used as the solvent for the equilibrated solution of β-Car and AEM(II) salts and Kaem.

The kinetics of DPPH˙ scavenging by AEM(II)–kaempferol complexes were investigated using a stopped-flow technique with the same method as previously performed on an RX2000 Rapid-Mixing Stopped-Flow Unit (Applied Photophysics Ltd, Surrey, United Kingdom).[5,6] For one syringe solution, DPPH˙ was dissolved in ethanol to obtain an absorbance of 0.92 ± 0.02 (extinction coefficient $\varepsilon = 9660$ L mol^{-1} cm^{-1}) at 516 nm,[32] and the final concentration of the DPPH˙ was calculated to be 100 μM. The other syringe solution was an equilibrated sample to be measured.

Quantum chemical calculations

Structural optimization of Kaem or Api and the AEM(II) were performed using the Gaussian 09 package and self-consistent reaction field (SCRF) model with the Becke3 and Lee Yang Parr (B3LYP) hybrid functional method along with Def2-SVP basis set.[33]

The proton dissociation enthalpy (PDE), ionization potential (IP) and bond dissociation enthalpy (BDE) of both Kaem and Api and their AEM(II) complexes were calculated as the gas phase enthalpy difference:

$$\text{Ar-OH} \rightarrow \text{Ar-O}^{\cdot} + \text{H}^{\cdot}$$

$$\text{Ar-OH} \rightarrow \text{Ar-O}^{-} + \text{H}^{+}$$

$$\text{Ar-OH} \rightarrow \text{Ar-OH}^{\cdot+} + \text{e}$$

$$\text{Ar-O}^{-} \rightarrow \text{Ar-O}^{\cdot} + \text{e}$$

Ar represents an unsaturated group linked to hydroxyl in Kaem or Api and their AEM complexes. Enthalpies of H˙ (-312.88 kcal mol^{-1}) and H^+ (1.48 kcal mol^{-1}) were also calculated, and the enthalpy of an electron (0.75 kcal mol^{-1}) was obtained from literature.[34]

Dihedral angles (α) between the two planes of the two Kaem ligands in complexes were calculated according to eqn (1):

$$\cos\langle\boldsymbol{\alpha}\rangle = \frac{\vec{m}\cdot\vec{n}}{\sqrt{\vec{m}^2 + \vec{n}^2}} \quad (1)$$

in which, $\vec{m}$ and $\vec{n}$ represent two normal vectors of two Kaem planes, respectively. $\vec{m}(A_1, B_1, C_1)$ and $\vec{n}(A_2, B_2, C_2)$ were obtained from the following two equations of two planes including metal ions and the two oxygen atoms within the same plane,

$$A_1x + B_1y + C_1z + D_1 = 0 \quad (2)$$

and

$$A_2x + B_2y + C_2z + D_2 = 0 \quad (3)$$

in which, (A_1, B_1, C_1) and (A_2, B_2, C_2) represent two normal vectors $\vec{m}$ and $\vec{n}$, and x, y, z represent the coordinates of optimized metal ions and the four oxygen atoms in two Kaem planes coordinated to metal ions, and D_1 and D_2, are constants, respectively.

Results

Reactions of AEM(II) ions with Kaem or Api and the formation of complexes

The UV-vis absorption spectra of 20 μM of Kaem with a maximum absorption at 368 nm in ethanol clearly shifted to the long wavelength region by addition of Mg/Ca/Sr/Ba(II) ions, as seen in Fig. 1a–d. Addition of 2 to 20 μM Mg(II) ions to Kaem showed a similar spectral shift to around 425 nm upon the addition of the heavier AEM(II) ions Ca/Sr/Ba(II). Further addition of up to 30 μM of Mg(II) ions to Kaem resulted in a further red shift and the formation of a new species with a maximum peak at 445 nm, while no further red shift occurred upon the addition of even excessive concentrations of Ca/Sr/Ba(II) ions to Kaem solution. Both Mg(II)–kaempferol complexes were found to have very similar characteristics in terms of their absorption spectra and Jobs plot (Fig. 1a, inset), as also observed for 1 : 1 Zn(II)–Kaem and 1 : 2 Zn(II)–$Kaem_2$ binding at the 3-hydroxyl and 4-carbonyl groups in our recent study.[5]

The same method of deconvolution and calculations of the equilibrium distribution between the two species as used for the Zn(II)–Kaem complexes in ref. 5, gave 1 : 1 cationic Mg(II)–$(Kaem–H)^+$ and 1 : 2 neutral Mg(II)–$(Kaem–H)_2$ complexes (Scheme 1c and d) with maximum absorption peaks at 445 and 425 nm (Fig. 2a), formed from the binding of Mg(II) to Kaem at the 3-hydroxyl and 4-carbonyl groups, resulting in the deprotonation of the 3-hydroxyl group, as shown in eqn (4) and (5). The 1 : 1 Mg(II)–kaempferol complex was found to transform into a 1 : 2 Mg(II)–kaempferol complex upon the addition of acetic acid (Fig. S1†), which indicates that the most stable 1 : 1 Mg(II)–kaempferol complex is neutral, Mg(II)–(Kaem–2H) (Scheme 1e), formed from the spontaneous deprotonation of cationic Mg(II)–$(Kaem–H)^+$ due to the increased acidity of phenol upon Mg(II) coordination. This result is also supported by the calculated proton deprotonation enthalpy (PDE) values and will be further explained in the *Structural and thermodynamic analyses* section. The formation of the 1 : 1 and 1 : 2 complexes and the transformation of the two complexes are shown in eqn (4)–(6):

$$\text{Mg(II)} + \text{Kaem} \overset{-\text{H}^+, K_1}{\rightleftharpoons} \text{Mg} - (\text{Kaem} - \text{H})^+ \quad (4)$$

$$\mathrm{Mg(II)} + 2\mathrm{Kaem} \overset{-2\mathrm{H}^+, K_2}{\rightleftharpoons} \mathrm{Mg} - (\mathrm{Kaem} - \mathrm{H})_2 \quad (5)$$

$$2\mathrm{Mg(II)}\text{–}(\mathrm{Kaem}\text{–}2\mathrm{H}) + 2\mathrm{H}^+ \rightleftharpoons \mathrm{Mg(II)}\text{–}(\mathrm{Kaem}\text{–}\mathrm{H})_2 + \mathrm{Mg(II)} \quad (6)$$

For convenience, the formulae Mg(II)–Kaem$^+$ and Mg(II)–Kaem are used to represent the 1 : 1 cationic Mg(II)–(Kaem–H)$^+$ and the neutral Mg(II)–(Kaem–2H) complexes, respectively. The 1 : 2 Mg(II)–Kaem complex is neutral, formed by the loss of a proton from each of the 3-hydroxyl groups of the two Kaem ligands, and is written as Mg(II)–Kaem$_2$. The stability constants were calculated to be 8.8×10^4 L mol^{-1} for Mg(II)–Kaem and 1.9×10^{10} L^2 mol^{-2} for Mg(II)–Kaem$_2$ in ethanol. A similar binding pattern was also observed in ethanol : chloroform (7 : 3, v/v), and stability constants were 1.9×10^4 L mol^{-1} for Mg(II)–Kaem and 3.2×10^{10} L^2 mol^{-2} for Mg(II)–Kaem$_2$.

Absorption spectra (Fig. 1b–d) and the derived Job plots (Fig. 1b–d insets) resulting from addition of the heavier AEM(II) ions Ca/Sr/Ba(II) to Kaem indicate only 1 : 2 M(II)–Kaem$_2$ (M = Ca, Sr, Ba) complexes formed, with a shoulder peak at 425 nm, as seen in eqn (7) and Fig. 2b. The obtained stability constants for Ca/Sr/Ba(II)–Kaem$_2$, 4.9×10^9/2.4×10^{10}/1.2×10^{10} L^2 mol^{-2} in ethanol, and 6.4×10^9/6.9×10^9/5.6×10^9 L^2 mol^{-2} in ethanol : chloroform (7 : 3, v/v), respectively, are listed in Table 1 together with the values for the 1 : 1 and 1 : 2 Mg(II)–kaempferol complexes.

$$\mathrm{M(II)} + 2\mathrm{Kaem} \overset{-2\mathrm{H}^+}{\rightleftharpoons} \mathrm{M(II)} - (\mathrm{Kaem} - \mathrm{H})_2,$$
$$\mathrm{M} = \mathrm{Ca(II)},\ \mathrm{Sr(II)},\ \mathrm{Ba(II)} \quad (7)$$

In contrast, only Mg(II) among the AEM(II) ions binds to apigenin (Api) (Fig. 1e and 2c). A shift to a lower wavenumber for the stretching vibration of the C=O double bond in the IR spectra (Table S1†) and the Job plot (Fig. 1e inset) characteristics indicate that the Mg(II) ions bind Api at the 4-carbonyl and 5-hydroxyl groups in a 1 : 1 stoichiometric ratio, forming a cationic Mg(II)–Api$^+$ complex, with the structure shown in Scheme 1f. Nevertheless, no reaction occurred between the Ca/Sr/Ba(II) ions and Api, as evidenced by lack of spectral changes both in the UV-vis and IR absorption spectra following the

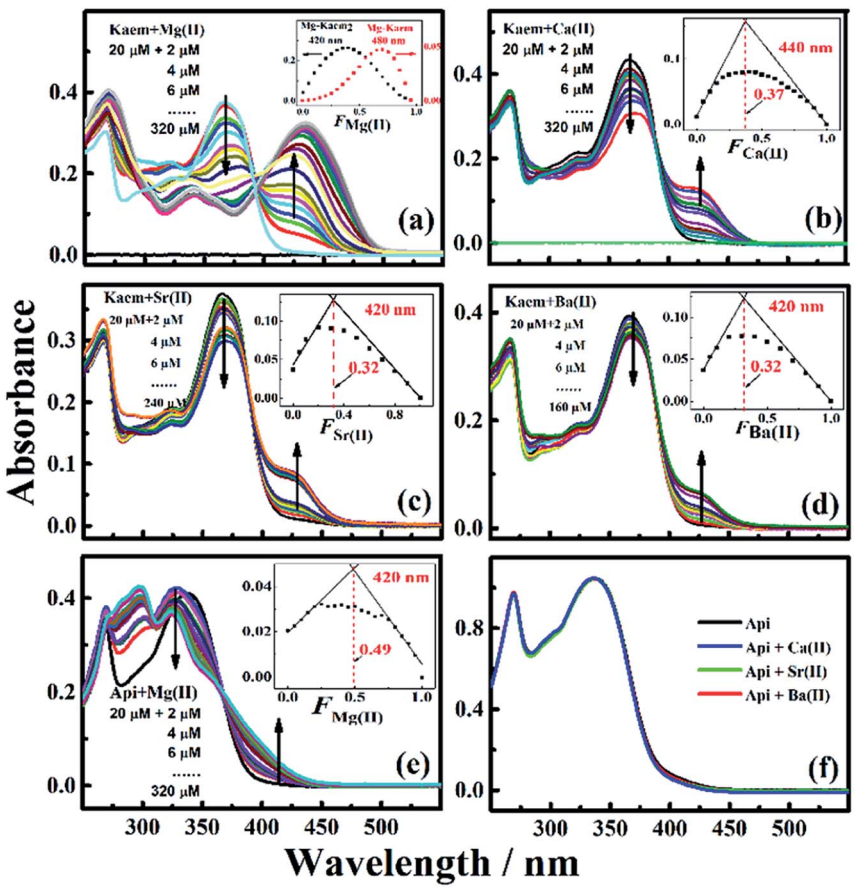

Fig. 1 Absorption spectra of 20 μM Kaem and solutions of 20 μM Kaem with (a) $Mg(CH_3COO)_2$, (b) $Ca(CH_3COO)_2$, (c) $Sr(CH_3COO)_2$ and (d) $Ba(CH_3COO)_2$ in the concentration range of 2 to 320 μM, and the absorption spectra of (e) 20 μM Api and solutions of 20 μM Api with $Mg(CH_3COO)_2$ in the same concentration range, and spectra of (f) 50 μM Api and solutions of 50 μM Api with 1000 μM of $Ca(CH_3COO)_2$, $Sr(CH_3COO)_2$ and $Ba(CH_3COO)_2$, respectively. Insets in (a–e): Job plots derived from the spectra at the indicated wavelengths for Kaem or Api with AEM(II) acetates in a total concentration of 50 μM in different ratios varying from 19 : 1 to 1 : 19 in (a), (b) and (e), and from 9 : 1 to 1 : 9 in (c) and (d). The solvent used was ethanol.

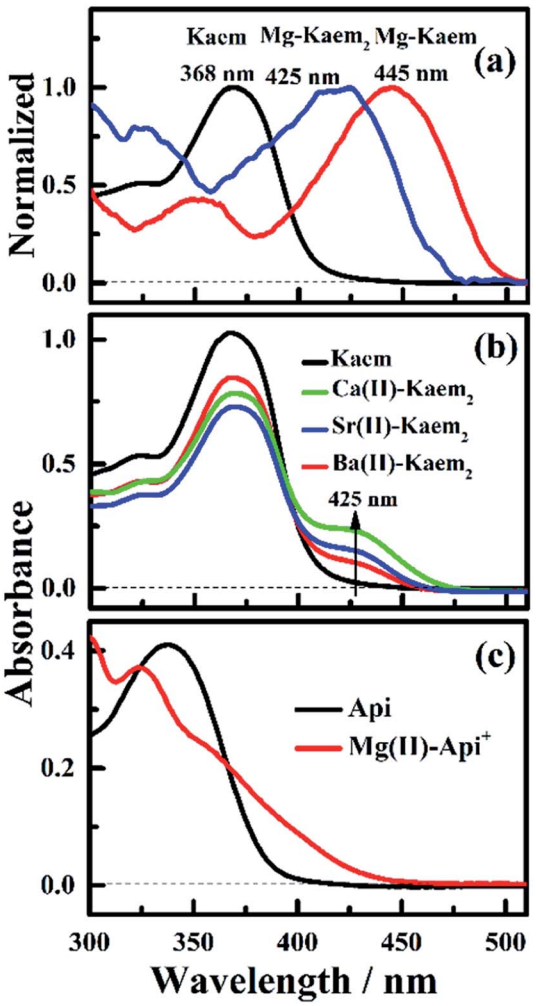

Fig. 2 (a) Normalized absorption spectra of Kaem and deconvoluted spectra of the 1 : 2 Mg(II)–$Kaem_2$ and neutral 1 : 1 Mg(II)–Kaem complexes. Absorption spectra of (b) the 50 μM Kaem and deconvoluted spectra of Ca(II)–$Kaem_2$, Sr(II)–$Kaem_2$ and Ba(II)–$Kaem_2$ complexes from solutions containing 50 μM of Kaem and 2000 μM of $Ca(CH_3COO)_2$, $Sr(CH_3COO)_2$ and $Ba(CH_3COO)_2$, respectively, and of (c) 20 μM of Api and deconvoluted spectra of Mg(II)–Api^+ from the solution containing 20 μM of Api and 320 μM of $Mg(CH_3COO)_2$.

addition of Ca/Sr/Ba(II) ions to Api solution (Fig. 1f and Table S1†). These observations support Ca/Sr/Ba(II) ion bonding with Kaem at the 3-hydroxyl and 4-carbonyl groups of the C-ring, as in the Mg(II)–Kaem complexes. The structures of the AEM(II)–kaempferol and Mg(II)–apigenin complexes are shown in Scheme 1c–f. Mass spectrometry (Tables S2†) further confirmed the composition obtained from the UV-visible spectra of the four 1 : 2 AEM(II)–$Kaem_2$ complexes and the 1 : 1 Mg(II)–Kaem and Mg(II)–Api^+ complex.

Determinations of oxidation potentials

A significant decrease in the oxidation potential of 50 μM of Kaem from 0.166 to −0.044 V *versus* ferrocene from the CV scan was observed following the addition of Mg(II) to Kaem with a Kaem :Mg (II) ratio ranging from 1 : 0.2 to 1 : 20 in ethanol/chloroform (7/3, v/v), as shown in Fig. 3a. Oxidation potentials obtained from the initial oxidation peak corresponded to the oxidation of phenolic groups.[37,38] The potential for the 1 : 1 Mg(II)–Kaem complex was estimated to be at −0.044 V, as obtained from a sample of Kaem and Mg(II) in ratio of 1 : 20 with 62% of the 1 : 1 Mg(II)–Kaem complex dominating in equilibrium with 3% Kaem and 35% Mg(II)–$Kaem_2$, as shown in Table S3.† The decrease in oxidation potential for the solutions with increasing addition of Mg(II) was found to have a similar tendency as the increase in the fraction of 1 : 1 Mg(II)–Kaem, as shown in Fig. 3b, excluding the contribution of 1 : 2 Mg(II)–$Kaem_2$ to the decrease in the oxidation potential. The oxidation potential of the 1 : 2 Mg(II)–$Kaem_2$ complex was estimated as 0.153 V for the combination of Kaem : Mg(II) = 1 : 0.2 with 34% of Mg(II)–$Kaem_2$ present in equilibrium with 64% Kaem and 2% 1 : 1 Mg(II)–Kaem, which is close to values for the parent Kaem and 1 : 2 Zn(II)–$Kaem_2$.

In addition, significant decreases in oxidation potentials were observed for combinations of Ca/Sr/Ba(II) ions and Kaem in ethanol/chloroform (7/3, v/v). The oxidation potentials were found to be at approximately −0.081 V for Ca(II)–$Kaem_2$, −0.084 V for Sr(II)–$Kaem_2$ and −0.098 V for Ba(II)–$Kaem_2$ as obtained from Kaem and Ca/Sr/Ba(II) ions in a ratio of 1 : 10 with >94% of 1 : 2 Ca/Sr/Ba(II)–$Kaem_2$ as the predominate components, see Fig. 3c and Table 1. The oxidation peak of 50 μM of Api is weak and has the approximate value of 0.409 V. No change in the oxidation potentials was observed for Api upon the addition of excess Mg(II), as shown in Fig. 3d.

Similar changes were also observed for AEM(II)–Kaem complexes in ethanol and the corresponding oxidation potentials were determined and are listed in Table 1.

Radical scavenging kinetics

Antioxidant activities of Kaem/Api, and of the complexes of Mg/Ca/Sr/Ba(II) with Kaem and of Mg(II) with Api were evaluated using the two radical scavenging methods as previously reported in the literature:[5] (i) scavenging of the photo-induced carotenoid radical cations β-$Car^{\bullet+}$ in ethanol/chloroform (7/3, v/v), which is now a well-established method for determining the radical scavenging of polyphenols and of Zn(II)–Kaem complexes *via* electron transfer (ET); and (ii) the scavenging of the semi-stable radical $DPPH^{\bullet}$ in ethanol, which has now has been accepted to occur *via* hydrogen atom transfer (HAT) from polyphenolic antioxidants.[39]

(i) β-Carotene radical cation scavenging. The decay of β-$Car^{\bullet+}$, with an absorption at 940 nm, and the simultaneous recovery of β-Car absorption after initial bleaching at 510 nm following photolysis were found to not be affected by the presence of AEM(II) ions or by Kaem alone. It was found to be significantly accelerated by the addition of each of the four AEM(II) ions together with Kaem, as shown in Fig. 4a and c. A series of solutions with Kaem : Mg(II) at varying ratios from 1 : 0.2 to 1 : 5 were used to investigate the β-$Car^{\bullet+}$ scavenging reactivity of the 1 : 1 Mg(II)–Kaem and 1 : 2 Mg(II)–$Kaem_2$ complexes. Solutions of Kaem with an excess of AEM(II) ions were used for investigating the combinations of Kaem and Ca/

Table 1 Radius and polarization of metal ions, Mg/Ca/Sr/Ba(II), coordination ratios and binding sites of metal ions with kaempferol (Kaem) and apigenin (Api). Stability constants K_1 (L mol^{-1}) and K_2 (L^2 mol^{-2}) and oxidation potentials (E) in ethanol (eth) and in ethanol : chloroform (eth : chl, 7/3), and absolute second order rate constants $k_{Car^{\bullet+}}$(L mol^{-1} s^{-1}) for the scavenging of β-Car$^{\bullet+}$ and $k_{DPPH^{\bullet}}$(L mol^{-1} s^{-1}) for the scavenging of DPPH$^{\bullet}$ by metal–flavonoid complexes. The parameters of Zn(II)–kaempferol complexes are shown for comparison

Flav	Metal ions	r^a (pm)	Polarization^b	M(II) : Flav	Binding site	K_1/K_2^{eth}, 1 : 1 (L mol^{-1})/ 1 : 2 (L^2 mol^{-2})	$K_1/K_2^{eth:chl}$, 1 : 1 (L mol^{-1})/1 : 2 (L^2 mol^{-2})	E^{eth} (V)	$E^{eth:chl}$ (V)	$k_{Car^{\bullet+}}$ (L mol^{-1} s^{-1})	$k_{DPPH^{\bullet}}$ (L mol^{-1} s^{-1})
Kaem	Zn(II)^c	74	5.41	1 : 1	3,4	4.8×10^5	1.0×10^5		−0.097	$(1.88 \pm 0.05) \times 10^8$	$(2.5 \pm 0.03) \times 10^4$
				1 : 2	3,4	1.2×10^{11}	2.0×10^{10}		0.170		$(1.3 \pm 0.07) \times 10^4$
	Ca(II)	99	4.04	1 : 2	3,4	4.9×10^9	6.4×10^9	−0.093	−0.081	$(5.44 \pm 0.02) \times 10^8$	$(2.9 \pm 0.02) \times 10^5$
	Sr(II)	113	3.54	1 : 2	3,4	2.4×10^{10}	6.9×10^9	−0.096	−0.084	$(3.38 \pm 0.02) \times 10^8$	$(8.1 \pm 0.01) \times 10^4$
	Ba(II)	135	2.96	1 : 2	3,4	1.2×10^{10}	5.6×10^9	−0.122	−0.098	$(3.17 \pm 0.02) \times 10^8$	$(1.3 \pm 0.03) \times 10^5$
Api	Mg(II)	65	6.15	1 : 1	4,5	2.4×10^5		0.409			

^{a} From ref. 35. ^{b} From ref. 36. ^{c} Formation constants, oxidation potentials (solvent is methanol : chloroform = 7 : 3) and rate constants are from ref. 5.

Sr/Ba(II), with the 1 : 2 Ca/Sr/Ba(II)–Kaem$_2$ complexes dominating. Notably, the decay of β-Car$^{\bullet+}$ by Kaem became notably faster upon the addition of AEM(II) ions compared to previously reported[5] results in which the same amount of Zn(II) was added, while the absorbance amplitudes for the bleaching recovery of the β-Car ground state were smaller. These results together imply that other reactions than ET to β-Car$^{\bullet+}$ occur for the AEM(II)–Kaem complexes as the reaction products do not completely return to the ground state of β-Car. Stronger absorbances were observed at 940 nm for the solutions of Kaem with Ca/Sr/Ba(II) ions than for the solutions of only Kaem or of each of the AEM(II) ions, especially for the combinations of Kaem and Sr/Ba(II) (Fig. 4c). The fast decay of β-Car$^{\bullet+}$ without full recovery of the β-Car ground state molecule was also observed for tea polyphenols and *m*-hydroxybenzoic acid in our previous studies and has been ascribed to the formation of radical adducts.[40,41] The scavenging of β-Car$^{\bullet+}$ in the present study seems accordingly to include both β-Car$^{\bullet+}$ reduction to β-Car upon accepting an electron from AEM(II)–Kaem complexes, and addition of AEM(II)–Kaem complexes to β-Car$^{\bullet+}$, as shown in eqn (8) and (9):

$$\beta\text{-Car}^{\bullet+} + \text{AEM(II)} - \text{kaempferol} \xrightarrow{k_2^{ET}} \beta\text{-Car} + \text{AEM(II)} - \text{kaempferol}^{\bullet+} \quad (8)$$

$$\beta\text{-Car}^{\bullet+} + \text{AEM(II)} - \text{kaempferol} \xrightarrow{k_2^{addition}} [\beta\text{-Car}\cdots\text{AEM(II)} - \text{kaempferol}]^{\bullet+} \quad (9)$$

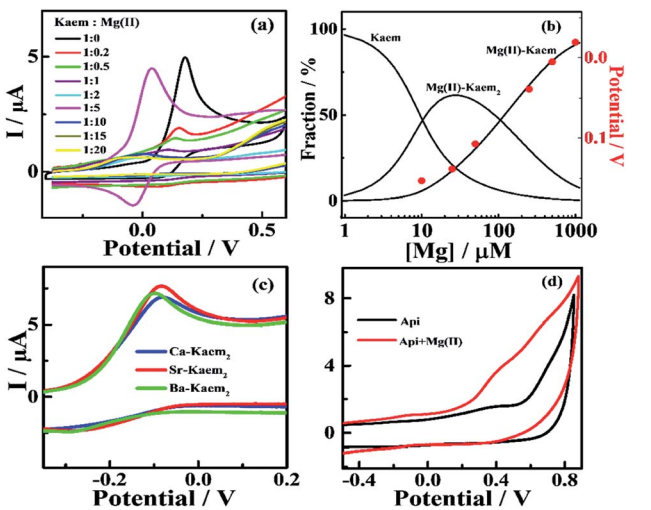

Fig. 3 CVs of (a) 50 μM of Kaem and solutions of 50 μM of Kaem with 10, 25, 50, 100, 250, 500, 750 and 1000 μM of $Mg(CH_3COO)_2$, (c) solutions of 100 μM of Kaem with 1000 μM of Ca(II), Sr(II) and Ba(II), and (d) 100 μM of Api and solutions of 100 μM of Api with 1000 μM of Mg(II), relative to 50 μM of ferrocene in 0.10 M $NaClO_4$, recorded at a scan rate of 0.05 V s^{-1}. (b) Oxidation potentials obtained from (a) (red circles) and molar fractions (solid lines) of Kaem and deconvoluted 1 : 2 Mg(II)–Kaem$_2$ and 1 : 1 Mg(II)–Kaem against the concentration of $Mg(CH_3COO)_2$ calculated from formation constants, $K_1 = 1.9 \times 10^4$ L mol^{-1} and $K_2 = 3.2 \times 10^{10}$ L^2 mol^{-2}. The solvent used was ethanol/chloroform (7/3, v/v).

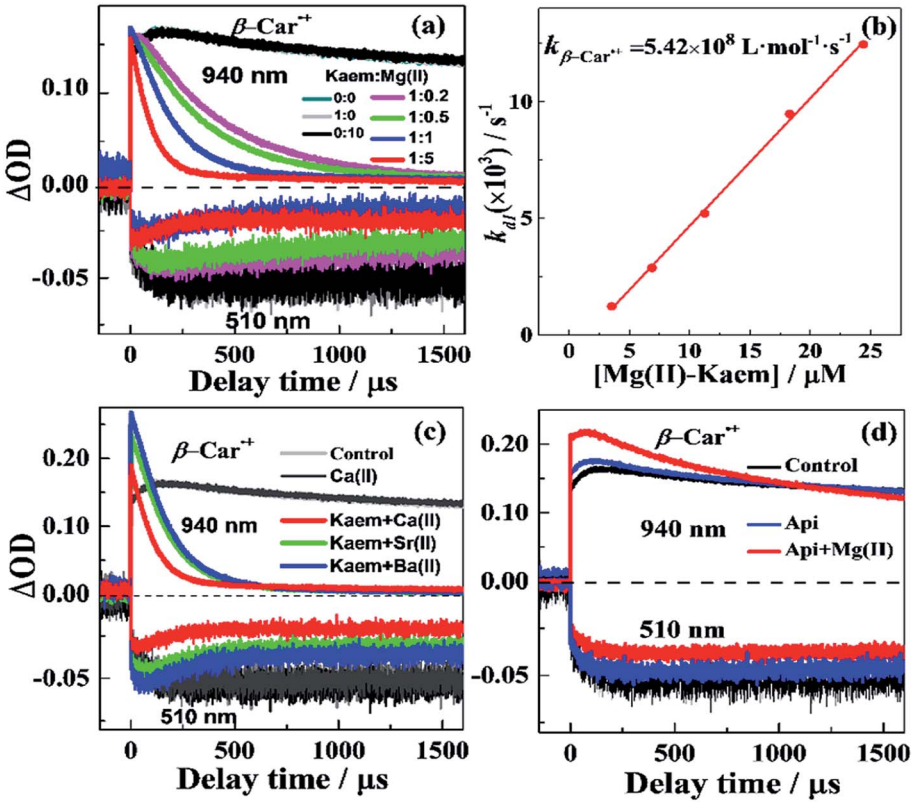

Fig. 4 Decay of β-Car$^{\bullet+}$ as monitored at 940 nm and the bleaching recovery of the β-Car ground state at 510 nm (a) in the absence and presence of 50 μM of Kaem and of 50 μM of Kaem with 10, 25, 50, and 250 μM of $Mg(CH_3COO)_2$, (c) in the presence of 50 μM of Kaem with 500 μM of $Ca(CH_3COO)_2$, $Sr(CH_3COO)_2$, $Ba(CH_3COO)_2$, and (d) in the absence and presence of 50 μM of Api and of 50 μM of Api with 750 μM of $Mg(CH_3COO)_2$. Kinetics with only β-Car and with only β-Car and AEM acetate salts were also investigated and are shown for comparison. (b) Observed rate constants obtained from exponential fitting of the fast decay of β-Car$^{\bullet+}$ (k_{d1}, Table 2) at 940 nm in (a) against the concentration of $Mg(CH_3COO)_2$. The second-order rate constant for the 1 : 1 Mg(II)–Kaem scavenging of β-Car$^{\bullet+}$ was calculated to have the value $k_{\beta\text{-Car}^{\bullet+}} = (5.42 \pm 0.04) \times 10^8$ L mol^{-1} s^{-1} by linear regression. The solvent used was ethanol/chloroform (7/3) and measurements were made at 25 °C.

The radical adduct observed at 940 nm was a reaction intermediate, which further dissociated into a final product, as evidenced by the absence of absorption in the near-infrared region (870 to 950 nm) after 532 nm laser radiation for 5 min of the solutions of β-Car and the AEM(II)–Kaem complexes (Fig. S2†). The kinetics observed for the absorption at 940 nm for all

Table 2 Time constants (τ), rate constants (k) and amplitudes (A) of the fast exponential increase (τ_i, k_i, A_i) and the di-exponential decay (τ_{d1}, τ_{d2}, k_{d1}, k_{d2}, A_{d1}, A_{d2}) at 940 nm and the fast formation (τ_f, k_f, A_f) and slow recovery (τ_r, k_r, A_r) of bleaching at 510 nm from the kinetic curves of Fig. 4 for solutions of β-Car and AEM(II)–Kaem complexes in ethanol/chloroform (7 : 3, v/v)

		Mg(II) + Kaem				$Ca(II)–Kaem_2$	$Sr(II)–Kaem_2$	$Ba(II)–Kaem_2$
λ/nm	Fitting parameters	1 : 0.2	1 : 0.5	1 : 1	1 : 5	1 : 10	1 : 10	1 : 10
940 nm	τ_i/μs	40.0	41.1	37.4	25.4	26.9	35.0	38.2
	$k_i(\times10^4)/s^{-1}$	2.5	2.4	2.7	3.9	0.037	0.029	0.026
	A_i	−0.032	−0.031	−0.032	−0.026	−0.026	−0.050	−0.054
	τ_{d1}/μs	402.3	320.3	175.3	86.8	96.7	150.3	149.9
	$k_{d1}(\times10^3)/s^{-1}$	2.5	3.1	5.7	12	1000	6.7	6.7
	A_{d1}	0.17	0.17	0.18	0.17	0.20	0.27	0.30
	τ_{d2}/μs	4285	4613	4263	3286	2705	1801	1303
	$k_{d2}(\times10^2)/s^{-1}$	2.3	2.2	2.3	3.0	3.7	5.6	7.7
	A_{d2}	0.017	0.014	0.015	0.014	0.012	0.011	0.012
510 nm	τ_f/μs	16.0	17.6	8.8	34.7	4.4	79.1	73.0
	$k_f(\times10^4)/s^{-1}$	6.3	5.7	11	2.9	23	1.3	1.4
	A_f	−0.030	−0.027	−0.023	−0.019	−0.024	−0.031	−0.040
	τ_r/μs	1868	860	338	76	135.6	170.4	153.4
	$k_r(\times10^3)/s^{-1}$	0.54	1.2	3.0	13	7.4	509	6.5
	A_r	−0.013	−0.015	−0.014	−0.025	−0.014	−0.040	−0.049

samples could be accommodated by a tri-exponential function $A_i e^{-t/\tau^i} + A_{d1}(1 - e^{-t/\tau_{d1}}) + A_{d2}(1 - e^{-t/\tau_{d2}})$, including a fast increase ($\tau_{i,}$ k_i), a relatively fast and dominating decay (τ_{d1}, k_{d1}), and a slower minor decay (τ_{d2}, k_{d2}), as shown in Table 2. For the combination of Kaem and Mg(II), k_{d1} accounting for >90% amplitude of the decay was found to be linearly dependent on the concentration of the 1 : 1 Mg(II)–Kaem complex present, as calculated from the formation constants (Fig. 4b). The 1 : 1 Mg(II)–Kaem complex was accordingly confirmed to be the only β-Car$^{\bullet+}$ radical scavenger and the 1 : 2 Mg(II)–Kaem complex was non-reactive in β-Car$^{\bullet+}$ scavenging. The second order rate constant was found to have the value $k_{Car^{\bullet+}} = (5.42 \pm 0.04) \times 10^8$ L mol^{-1} s^{-1}, as obtained by the linear fitting of the observed pseudo first-order rate constant k_{d1} against the concentration of the 1 : 1 Mg(II)–Kaem (Fig. 4b and Table 1). For combinations of Kaem with Ca(II), Sr(II) or Ba(II), for which the results are shown in Fig. 4c, the second order rate constants $k_{Car^{\bullet+}}$ were obtained from the observed pseudo first-order rate constant k_{d1} by division with the concentration of the 1 : 2 Ca/Sr/Ba(II)–Kaem$_2$ complex as the only complex formed and accordingly as the only β-Car$^{\bullet+}$ radical scavenger present. The second order rate constant for the decay of β-Car$^{\bullet+}$ by the AEM complexes was the largest for 1 : 2 Ca(II)–Kaem$_2$, with the value (5.44 ± 0.02) × 10^8 L mol^{-1} s^{-1}, as compared with the 1 : 1 Mg(II)–Kaem complex with the value (5.24 ± 0.04) × 10^8 and with (3.38 ± 0.02) × 10^8 L mol^{-1} s^{-1} for Sr(II)–Kaem$_2$ and (3.17 ± 0.02) × 10^8 L mol^{-1} s^{-1} for Ba(II)–Kaem$_2$, where a quantitative comparison is shown in Fig. 5a.

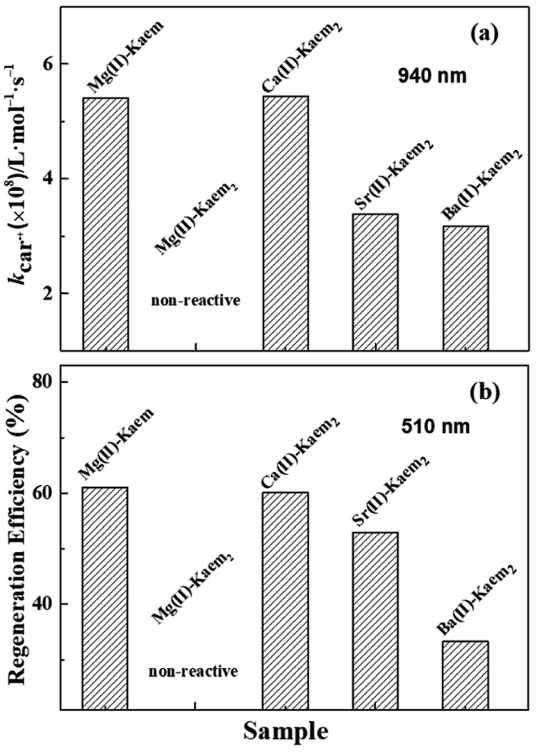

Fig. 5 (a) Second-order rate constants of β-Car$^{\bullet+}$ scavenging by 1 : 1 Mg(II)–Kaem and by 1 : 2 Ca/Sr/Ba(II)–Kaem$_2$ complexes obtained from the linear fitting of pseudo first-order rate constants at 940 nm, as shown in Fig. 4a and c. (b) Regeneration efficiency of β-Car$^{\bullet+}$ to yield β-Car by the 1 : 1 Mg(II)–Kaem and 1 : 2 Ca/Sr/Ba(II)–Kaem$_2$ complexes, as obtained from amplitude ratios of the bleaching kinetics at 510 nm in the presence and absence of the complexes in Fig. 4a and c.

The time constants and rate constants of the formation and recovery of bleaching at 510 nm for all AEM(II)–Kaem complexes could be accommodated by a di-exponential function $A_f e^{-t/\tau_f} + A_r(1 - e^{-t/\tau_r})$, including a fast formation ($\tau_{f,}$ k_f) without recovery and a subsequently slow recovery ($\tau_{r,}$ k_r), as shown in Table 2. The recovery at 510 nm for all complexes was found to be slower than the decay at 940 nm, which implies that the decay of β-Car$^{\bullet+}$ at 940 nm only partially regenerates to the β-Car ground state, further supporting the presence of an additional reaction that occurs for the decay of β-Car$^{\bullet+}$ formed by laser flash photolysis. The fraction of β-Car$^{\bullet+}$ regenerated by electron transfer was quantified using the ratios of the absorbance of β-Car bleaching at 510 nm at a longer delay time between the samples in the presence and absence of the complexes, as shown in Fig. 5b. The results indicate that the 1 : 1 Mg(II)–Kaem and 1 : 2 Ca(II)–Kaem$_2$ complexes are the most efficient radical scavengers that regenerate β-Car from β-Car$^{\bullet+}$ compared to 1 : 2 Sr(II)–Kaem$_2$ and Ba(II)–Kaem$_2$ (Fig. 5a and b). β-Car regeneration efficiency was 61% for 1 : 1 Mg(II)–Kaem, 60% for 1 : 2 Ca(II)–Kaem$_2$, 53% for Sr(II)–Kaem$_2$ and 33% for Ba(II)–Kaem$_2$, all of which are lower than the 87% for 1 : 1 Zn(II)–Kaem.

In contrast, Api alone had no effect on the decay of β-Car$^{\bullet+}$ and the combination of Mg(II) and Api only slightly accelerated the decay of β-Car$^{\bullet+}$, as evidenced by the higher absorbance at 940 nm in the presence of complexes than for only β-Car, with no recovery of the bleaching at 510 nm, as shown in Fig. 4d.

(ii) DPPH$^{\bullet}$ scavenging. Semi-stable DPPH$^{\bullet}$ scavenging was investigated for combinations of Kaem and AEM(II) ions as well as of Api and Mg(II) in ethanol monitored at 516 nm using stopped-flow spectroscopy, as shown in Fig. 6a–c. Upon the addition of 50 μM of Kaem to a 100 μM DPPH$^{\bullet}$ solution, the decay in the absorbance was clearly accelerated, whereas no effect was observed upon the addition of up to 1000 μM of Mg/Ca/Sr/Ba(II) alone. However, the rate of DPPH$^{\bullet}$ scavenging by Kaem was significantly accelerated upon the addition of AEM(II) ions, as can be seen in Fig. 6a and b.

For the combination of Kaem and Mg(II) in DPPH$^{\bullet}$ scavenging, the reaction rate depends on three parallel reactions of Kaem in equilibrium with the 1 : 1 and 1 : 2 Mg(II)–Kaem complexes. Individual second order rate constants, $k_2^{Kaem} = (1.59 \pm 0.01) \times 10^3$ L mol^{-1} s^{-1}, $k_2^{Mg(II)Kaem} = (3.5 \pm 0.03) \times 10^4$ L mol^{-1} s^{-1} and $k_2^{Mg(II)Kaem_2} = (3.4 \pm 0.03) \times 10^3$ L mol^{-1} s^{-1} were calculated from the distributions of Kaem, 1 : 1 Mg(II)–Kaem and 1 : 2 Mg(II)–Kaem$_2$ using the same method as for Zn(II)–kaempferol complexes to analyze the observed rate constant k_{obs} upon varying the Mg(II) : Kaem ratios (Table S3†). The asymmetric 1 : 1 Mg(II) Kaem was found to be 20 times and 10 times as efficient as the parent Kaem and symmetric 1 : 2 Mg(II)–Kaem$_2$ complex in DPPH$^{\bullet}$ scavenging, respectively.

For combinations of Kaem and the heavier AEM ions Ca/Sr/Ba(II), the reaction rates of DPPH$^{\bullet}$ scavenging depend on two parallel reactions of Kaem in equilibrium with the 1 : 2 Ca/Sr/

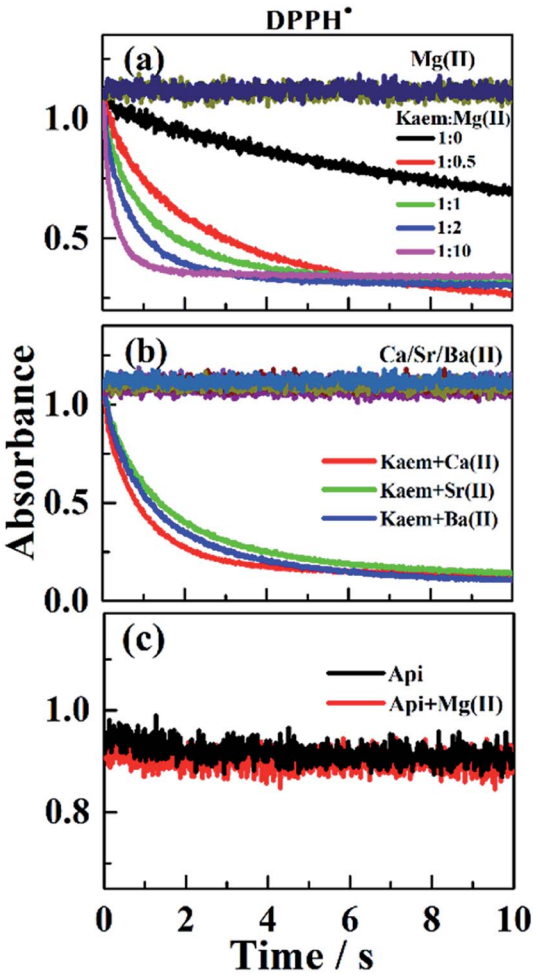

Fig. 6 Absorbances at 516 nm for DPPH• scavenged (a) by 50 μM of Kaem, by 1500 pf μM $Mg(CH_3COO)_2$, and by 50 μM of Kaem with 25, 50, 100, and 500 μM of $Mg(CH_3COO)_2$, and by (b) solutions containing 50 μM of Kaem with 25 μM of $Ca(CH_3COO)_2$, $Sr(CH_3COO)_2$ or $Ba(CH_3COO)_2$, respectively. $Ca(CH_3COO)_2$, $Sr(CH_3COO)_2$, $Ba(CH_3COO)_2$ up to 1.5 M had no effect on the kinetics of DPPH• scavenging, as shown for comparison. (c) Absorbances for the DPPH• kinetics were not affected by 50 μM of Api, or by the presence of 50 μM of Api together with 500 μM of $Mg(CH_3COO)_2$. The solvent used was ethanol and measurements were made at 25 °C.

Ba(II)–$Kaem_2$ complexes. Individual second order rate constants were obtained as $(2.9 \pm 0.02) \times 10^5$, $(8.1 \pm 0.01) \times 10^4$, $(1.3 \pm 0.03) \times 10^5$ L mol^{-1} s^{-1} for the 1 : 2 Ca(II)–$Kaem_2$, Sr(II)–$Kaem_2$ and Ba(II)–$Kaem_2$ complexes, respectively, based on the distributions of the 1 : 2 Ca/Sr/Ba(II)–$Kaem_2$ complexes in equilibrium with Kaem, which indicates that the 1 : 2 metal–Kaem complexes of the heavier Ca/Sr/Ba(II) ions are far more efficient radical scavengers than the complexes of the lighter Mg(II) ion and the transition metal ion Zn(II) in reacting with DPPH• (Table 1). Ca(II)–$Kaem_2$ has the highest scavenging rate constant, ~3.6 times that of Sr(II)–$Kaem_2$, 2.2 times that of Ba(II)–$Kaem_2$, 8 times that of 1 : 1 Mg(II)–Kaem, 85 times that of 1 : 2 Mg(II)–$Kaem_2$, and 182 times that of the parent Kaem. In contrast, no effect on the kinetics of DPPH• decay was observed upon the addition of Api or solutions of Api together with Mg(II), as can be seen in Fig. 6c.

A proposed mechanism for Kaem and Api scavenging of DPPH• in the presence and absence of AEM(II) ions and the radical scavenging activities of the AEM(II)–Kaem and Mg(II)–Api complexes are outlined in Scheme 2.

Structural and thermodynamic analyses

Molecular structures of the AEM(II)–Kaem and Mg(II)–Api complexes were optimized using density functional theory (DFT) methods, and the structural parameters are listed in Table 3. The results indicate that the bond lengths of the metal ions and oxygen atoms in the 1 : 2 di-coordinated AEM(II)–$Kaem_2$ complexes increase along with an increase in the radii of the AEM(II) ions (Table 3). Mono-coordinated Mg(II) with Kaem or Api as a ligand is planar (*optimized structures not shown*), while the two Kaem ligands in the 1 : 2 di-coordinated AEM(II)–$Kaem_2$ complexes are arranged in staggered spatial structures different from the planar structure of the 1 : 2 Zn(II)–$Kaem_2$ complex, the structures of which are shown in Fig. S3.† The two Kaem planes in the 1 : 2 Ca(II)–$Kaem_2$ complex have the highest dihedral angle of 89° (almost vertical) among all the AEM–kaempferol complexes, followed by 84° for 1 : 2 Mg(II)–$Kaem_2$, 77° for Sr(II)–$Kaem_2$ and 75° for Ba(II)–$Kaem_2$, as can be seen in Fig. S3† and Table 3.

Thermodynamic parameters, including proton dissociation enthalpies (PDE), ionization potentials (IP), and bond dissociation energies (BDE) of the AEM(II)–Kaem and Mg(II)–Api complexes, as well as those for Kaem and Api for comparison were calculated by DFT and are listed in Table 3. The PDE values for the 1 : 1 Mg(II)–Kaem complex were found to be 3 to 5 kcal mol^{-1} lower than for the parent Kaem, which further supports that the 1 : 1 cationic Mg(II)–$Kaem^+$ easily loses a proton to form a more stable di-deprotonated neutral Mg(II)–Kaem complex, as observed for 1 : 1 Zn(II)–Kaem. In addition, the 1 : 1 Mg(II)–Kaem complex also shows a lower IP and lower BDE and is more reducing and is a better radical scavenger than the parent Kaem.

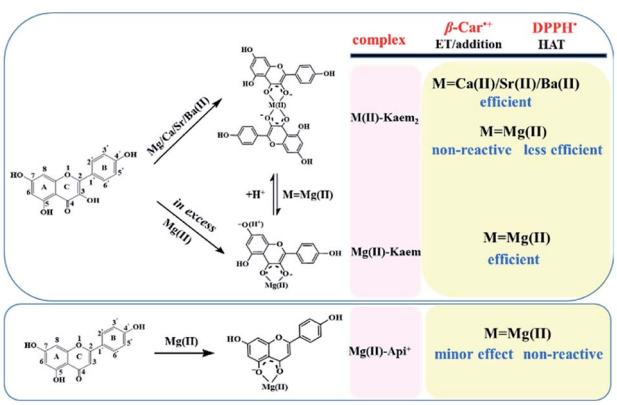

Scheme 2 Proposed mechanism for Kaem and for Api binding to AEM(II) ions and the radical scavenging activities of AEM(II)–Kaem and Mg(II)–Api complexes.

Table 3 Calculated bond lengths between the oxygen atom and AEM(II) ions L_{O-M} (Å), dihedral angle α (°) of the two ligands in the di-coordinated AEM(II)–$Kaem_2$ complexes, proton dissociation enthalpies (PDE), ionization potentials (IP), and bond dissociation enthalpy (BDE) of phenols in the parent Kaem and Api and the complexes, in kcal mol^{-1}

Compound	Group	Kaem	Mg–$Kaem^+$	Mg–Kaem[a]	Mg–$Kaem_2$	Ca–$Kaem_2$	Sr–$Kaem_2$	Ba–$Kaem_2$	Api	Mg–Api^+
L_{O-M} (Å)	3-O		1.95		1.98/1.98	2.32/2.32	2.52/2.52	2.79/2.79		
	4-O				2.04/2.04	2.42/2.42	2.60/2.60	2.89/2.90		
α (°)					84	89	77	75		
PDE (kcal mol^{-1})	5-OH	301.46	296.30		300.40	303.52	303.62	305.07	305.44	
	7-OH	295.27	292.26		294.81	296.51	296.93	297.59	296.09	294.37
	3-OH	297.81								
	4′-OH	297.06	294.89		297.72	299.57	299.87	300.62	295.35	295.71
IP (kcal mol^{-1})		126.55	178.66	107.56	114.71	114.51	111.55	107.01	133.86	185.82
BDE (kcal mol^{-1})	5-OH	89.99	84.93	84.72	84.91	83.36	80.94	80.53	94.33	—
	7-OH	87.11	82.91		81.10	77.94	76.36	74.47	88.96	90.93
	3-OH	76.69								
	4′-OH	81.54	79.72	74.82	77.90	74.84	73.46	71.66	84.79	86.10

[a] The IP and BDE values were calculated for neutral Mg–Kaem with the 7-phenol deprotonated as the most acidic phenol in the cationic Mg–$Kaem^+$ complex.

The PDE values in Table 3 of all four 1 : 2 AEM(II)–kaempferol complexes are almost unaffected compared to those of the parent Kaem or Api, while both the IP and BDE values decreased remarkably, especially for the 4′-phenol group in the B-ring, generally accepted as the most active group in contributing towards the antioxidant properties of the complexes. The BDE and IP values for 1 : 2 AEM(II)–$Kaem_2$ decreased in the order of: Mg(II) > Ca(II) > Sr(II) > Ba(II). In contrast, all the thermodynamic parameters, including the PDE, BDE and IP values of Api were not affected by the coordination of Mg(II).

Discussion

AEM ion complexes of Kaem and Api

The AEM ions differ dramatically in terms of their binding of Kaem and Api, despite their minor structural differences. Mg(II) binds to Kaem at the 3,4-site to form equilibrium mixtures of 1 : 1 and 1 : 2 Mg(II)–Kaem complexes and the parent Kaem, while Mg(II) binds with Api at the 4,5-site only forming a 1 : 1 Mg(II)–Api complex. Different from Mg(II), the heavier AEM(II) ions Ca/Sr/Ba(II) only form 1 : 2 AEM–$Kaem_2$ complexes at the 3,4-site, and no binding occurs between Ca/Sr/Ba(II) and Api. All four AEM(II) ions bind at the 3,4 site for Kaem, while Mg(II) only binds at the 4,5 site for Api. The absence of binding of Ca/Sr/Ba(II) with Api is in agreement with the fact that the 3-hydroxyl and 4-carbonyl groups are more preferential metal binding groups compared to the 4-carbonyl and 5-hydroxyl groups in flavonoids.[42,43] A smaller radius, higher polarization and accordingly stronger attraction to Kaem and Api for Mg(II) compared to Ca/Sr/Ba(II), but similar to Zn(II) as seen in Table 1, may explain the same coordination modes and similar spectra of the Mg(II)– and Zn(II)–Kaem complexes. Only in the presence of higher concentrations of Mg(II) or Zn(II), the 1 : 2 Mg(II)–$Kaem_2$ and Zn(II)–$Kaem_2$ complexes transform into the 1 : 1 Mg(II)–Kaem and Zn(II)–Kaem complexes *via* metal–oxygen cleavage. Due to the lower polarization of the heavier AEM(II) ions Ca/Sr/Ba(II) compared to Mg(II), no 1 : 1 Ca/Sr/Ba(II)–Kaem complexes were formed, even at high Ca/Sr/Ba(II) concentrations in Kaem solution, in agreement with that Ca/Sr/Ba(II) do not bind to Api in contrast to Mg(II) and Zn(II), which both bind with Api at the 4,5-site.

The absorption spectra of the four 1 : 2 AEM(II)–$Kaem_2$ complexes, obtained by deconvolution, all have new absorption bands at around 425 nm. The most intense absorption of the new spectral line is observed for Mg(II), followed by Ca(II), Sr(II), and Ba(II), corresponding to a decrease in polarization along with an increase in the metal ions radius. Among the AEM(II) ions, Mg(II) has the smallest radius, and accordingly the strongest polarization of the AEM(II)–$Kaem_2$ complexes, affecting the 3-hydroxyl and 4-carbonyl groups, resulting in a significant increase in the intensity of the new peak at 425 to 445 nm (Fig. 2a and b).

Radical scavenging of Kaem coordinated to AEM ions

Both the β-$Car^{\bullet+}$ and $DPPH^{\bullet}$ radical scavenging efficiencies of Kaem were significantly increased by the presence of any one of the four acetates of AEM(II), as evidenced by the scavenging rate both for the ultra-fast reactions determined using submicrosecond laser flash photolysis, and for the slower scavenging rates determined by stopped-flow techniques. Compared with the Zn(II)–Kaem complex, a faster formation of new species at the initial reaction time as seen in the near-infrared spectral region (940 nm) and a faster decay of β-$Car^{\bullet+}$ with less recovery of β-Car following bleaching (510 nm) for solutions of both AEM(II) and Kaem confirmed a parallel addition reaction in the ET reaction of the AEM(II)–Kaem complexes with β-$Car^{\bullet+}$. Based on the present results alone, it is, however, not possible to distinguish whether ET, hydrogen atom transfer (HAT) or an additional mechanism are the most important in the scavenging of $DPPH^{\bullet}$ by the AEM(II)–Kaem complexes. This was possible for β-$Car^{\bullet+}$ scavenging but not for the scavenging of $DPPH^{\bullet}$ by the AEM(II)–Kaem complexes due to the spectral overlaps with the final products. Absolute second reaction rate

constants of DPPH$^{\bullet}$ radical scavenging indicate, with the notable exception of Ca(II)–Kaem$_2$, that Ba(II)–Kaem$_2$ is the most efficient radical scavenger, followed by Sr(II)–Kaem$_2$, Mg(II)–Kaem, Mg(II)–Kaem$_2$, which strictly agrees with the hierarchy of their oxidation potentials, the BDE and the IP values in the order of: Ba(II)–Kaem$_2$ < Sr(II)–Kaem$_2$ < Mg(II)–Kaem < Mg(II)–Kaem$_2$ (Fig. 7). These data are consistent with the widely accepted HAT mechanism for DPPH$^{\bullet}$ scavenging by antioxidants.[37]

1 : 2 Mg(II)–Kaem$_2$ is non-reactive in β-Car$^{\bullet+}$ scavenging, as is the parent Kaem and the 1 : 2 Zn(II)–Kaem$_2$ complex, and is also the poorest DPPH$^{\bullet}$ radical scavenger among the AEM(II)–Kaem complexes studied. In contrast, its DPPH$^{\bullet}$ scavenging is fast compared to the parent Kaem, while the 1 : 2 Ca/Sr/Ba(II)–Kaem$_2$ complexes have increased scavenging rates for both radicals studied. These findings are consistent with the most positive oxidation potential determined electrochemically, and the calculated largest IP and BDE values for 1 : 2 Mg(II)–Kaem$_2$ (Fig. 7 and Table 3). The remarkable increase in radical scavenging efficiencies seen for the Ca/Sr/Ba(II)–Kaem$_2$ complexes may be understood by the increasing electron withdrawing capability of the $(n-1)$d orbital in the heavier AEM Ca(II), Sr(II) and Ba(II) ions, which accordingly makes them behave almost like transition metal ions, reducing the BDE and IP values of the ligand Kaem.[22] Such effects are not noted for Kaem coordinated to the lighter Mg(II) ion in 1 : 2 Mg(II)–Kaem$_2$. For both transition metal ions, Zn(II) and Cu(II), the 1 : 1 metal–flavonoid complex was previously found to have a higher radical scavenging ability as the result of asymmetric electron withdrawal from the phenolic group by the metal ions. In contrast, the 1 : 2 complexes, in which bi-coordinated flavonoid ligands symmetrically balance the electron withdrawal effect of the metal ion, were noted to show decreased radical scavenging ability.[5,6]

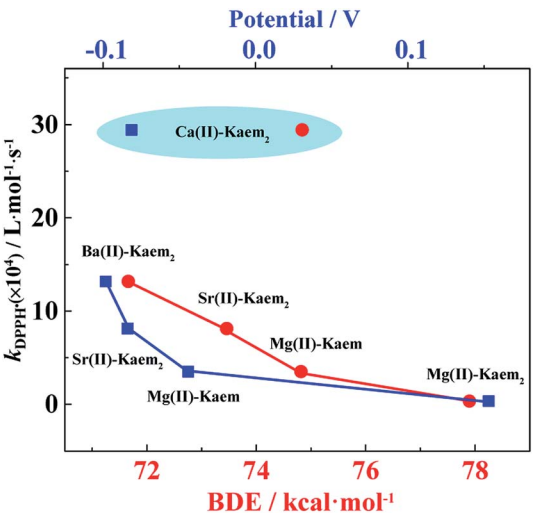

Fig. 7 Second order rate constants for DPPH$^{\bullet}$ scavenging by the AEM(II)–Kaem complexes (Mg, Ca, Sr, and Ba) dependent on the bond dissociation enthalpy, BDE (*lower axis*) and the oxidation potential (*upper axis*). Solid lines are only for guiding the eyes.

The 1 : 2 Ca(II)–Kaem$_2$ complex has a higher β-Car$^{\bullet+}$ and DPPH$^{\bullet}$ radical scavenging capacity than both the Sr(II)–Kaem$_2$ and Ba(II)–Kaem$_2$ complexes, although the thermodynamic parameters of 1 : 2 Ca(II)–Kaem$_2$, including experimentally determined oxidation potentials and calculated BDE and IP values, are less favorable than Sr(II)–Kaem$_2$ and Ba(II)–Kaem$_2$ (Fig. 7 and Table 3). Other factors must accordingly be important for radical scavenging. The dihedral angle of the two flavone backbones in Ca(II)–Kaem$_2$ is 89°, obviously larger than the 77° in Sr(II)–Kaem$_2$ and 75° in Ba(II)–Kaem$_2$. The lower steric hindrance in Ca(II)–Kaem$_2$ compared to other complexes may kinetically facilitate the formation and stability of a radical adduct both in the scavenging of β-Car$^{\bullet+}$ and DPPH$^{\bullet}$, and Ca(II)–Kaem$_2$ thus making it the most efficient radical scavenger. Ba(II)–Kaem$_2$ and Sr(II)–Kaem$_2$ are marginally less efficient in β-Car$^{\bullet+}$ radical scavenging reactivity than Ca(II)–Kaem$_2$, although they are thermodynamically more favorable.

The 1 : 1 mono-coordinated Mg(II)–Kaem complex has similar β-Car$^{\bullet+}$ scavenging reactivity as the 1 : 2 Ca(II)–Kaem$_2$ complex, but higher DPPH$^{\bullet}$ scavenging efficiency. This pattern could arise from the strong electron attraction by the polar Mg(II), increasing the radical scavenging efficiency of Kaem as a ligand, as clearly demonstrated for 1 : 1 Zn(II) and Cu(II) transition metal–flavonoid complexes.[5,6] However, 1 : 1 Mg(II)–Kaem is only formed in the presence of excessive concentrations of Mg(II) ions, and accordingly is of less significance in biological systems than the 1 : 2 Ca(II)–Kaem$_2$ complex.

For the 1 : 1 Mg(II)–Api complex, its formation shows an insignificant increase in β-Car$^{\bullet+}$ scavenging efficiency, and the complex formation has no effect on DPPH$^{\bullet}$ scavenging. A comparison of the Mg(II)–Kaem and Mg(II)–Api complexes indicates that Mg(II) binding at the 3-hydroxyl and 4-carbonyl groups is an important structural factor for promoting the radical scavenging efficiency of Kaem. 4-Carbonyl and 5-hydroxyl binding to the Mg(II) ions for Api and binding to the Cu(II) for genistein both have insignificant effects on the radical scavenging efficiencies of flavonoids.[18]

Conclusions

Coordination of kaempferol in 1 : 2 AEM(II)–Kaem$_2$ complexes by the heavier AEM(II) ions Ca(II), Sr(II) and Ba(II) increases the radical scavenging efficiency in contrast to binding to the lighter Mg(II) ion and to the transition metal ion Zn(II). This difference is suggested to be the result of the stronger electron withdrawing capability of the $(n-1)$d orbital in the heavier Ca(II), Sr(II) and Ba(II) ions compared to the lighter Mg(II) ion and the transitional metal ion Zn(II). Symmetry differences between the 1 : 1 and 1 : 2 complexes also increase the radical scavenging rate in favor of the 1 : 1 complexes, as observed for Zn(II). The Ca(II)–Kaem$_2$ complex is a far more efficient radical scavenger than the other AEM(II)– and Zn(II)–kaempferol complexes, and may accordingly find use as a food additive and an antioxidant, especially in dairy products with high calcium content. Based on the surprising findings for Kaem, calcium complexes of flavonoids should also be investigated as new metal-based drug candidates.

Abbreviations

AEM	Alkaline earth metal
Kaem	Kaempferol
Api	Apigenin
β-Car	β-Carotene
$\beta\text{-Car}^{\bullet+}$	β-Carotene radical cation
CV	Cyclic voltammetry
$DPPH^{\bullet}$	2,2-Diphenyl-1-picrylhydrazyl radical
ET	Electron transfer
DFT	Density functional theory
PDE	Proton dissociation energy
IP	Ionization potential
BDE	Bond dissociation energy

Conflicts of interest

There are no conflicts to declare.

Acknowledgements

This work was supported by grants from the Natural Science Foundation of China (Nos. 21573284 and 21673288).

References

1 P. G. Pietta, *J. Nat. Prod.*, 2000, **63**, 1035–1042.
2 W. Ngwa, R. Kumar, D. Thompson and W. Lyerly, *Molecules*, 2020, **25**, 2707.
3 S. Eghbaliferiz and M. Iranshahi, *Phytother. Res.*, 2016, **30**, 1379–1391.
4 D. Procházková, I. Boušová and N. Wilhelmová, *Fitoterapia*, 2011, **82**, 513–523.
5 Y. Xu, L.-L. Qian, J. Yang, R.-M. Han, J.-P. Zhang and L. H. Skibsted, *J. Phys. Chem. B*, 2018, **122**, 10108–10117.
6 Y. Xu, J. Yang, Y. Lu, L.-L. Qian, Z.-Y. Yang, R.-M. Han, J.-P. Zhang and L. H. Skibsted, *J. Phys. Chem. B*, 2020, **124**, 380–388.
7 M. M. Kasprzak, A. Erxleben and J. Ochocki, *RSC Adv.*, 2015, **5**, 45853–45877.
8 Y. Qi, M. Jiang, Y.-L. Cui, L. Zhao and S. Liu, *J. Hazard. Mater.*, 2015, **285**, 336–345.
9 M. Samsonowicz, E. Regulska and M. Kalinowska, *Chem.-Biol. Interact.*, 2017, **273**, 245–256.
10 S. Selvaraj, S. Krishnaswamy, V. Devashya, S. Sethuraman and U. M. Krishnan, *Med. Res. Rev.*, 2014, **34**, 677–702.
11 A. Raza, S. Bano, X. Xu, R. X. Zhang, H. Khalid, F. M. Iqbal, C. Xia, J. Tang and Z. Ouyang, *Biol. Trace Elem. Res.*, 2017, **178**, 160–169.
12 N. Ghosh, T. Chakraborty, S. Mallick, S. Mana, D. Singha, B. Ghosh and S. Roy, *Spectrochim. Acta, Part A*, 2015, **151**, 807–813.
13 Q. K. Panhwar and S. Memon, *J. Coord. Chem.*, 2011, **64**, 2117–2129.
14 A. Raza, X. Xu, L. Xia, C. Xia, J. Tang and Z. Ouyang, *J. Fluoresc.*, 2016, **26**, 2023–2031.
15 S. Roy, S. Mallick, T. Chakraborty, N. Ghosh, A. K. Singh, S. Manna and S. Majumdar, *Food Chem.*, 2015, **173**, 1172–1178.
16 Q. K. Panhwar, S. Memon and M. I. Bhanger, *J. Mol. Struct.*, 2010, **967**, 47–53.
17 M. Samsonowicz and E. Regulska, *Spectrochim. Acta, Part A*, 2017, **173**, 757–771.
18 J. Yang, Y. Xu, H.-Y. Liu, R.-M. Han, J.-P. Zhang and L. H. Skibsted, *Molecules*, 2017, **22**, 1757–1771.
19 Z.-Y. Yang, L.-L. Qian, Y. Xu, M.-T. Song, C. Liu, R.-M. Han, J.-P. Zhang and L. H. Skibsted, *Molecules*, 2020, **25**, 1975–1987.
20 G. Dehghan and Z. Khoshkam, *Food Chem.*, 2012, **131**, 422–426.
21 Q. K. Panhwar and S. Memon, *Inorg. Chim. Acta*, 2013, **407**, 252–260.
22 N. Sugihara, T. Arakawa, M. Ohnishi and K. Furuno, *Free Radical Biol. Med.*, 1999, **27**, 1313–1323.
23 K. Mai, R. Divyashree, G. Francesca and M. O. Helen, *Future Med. Chem.*, 2019, **11**, 2845–2867.
24 X. Wu, L. Zhao, J. Jin, S. Pan, W. Li, X. Jin, G. Wang, M. Zhou and F. Gernot, *Science*, 2018, **361**, 912–916.
25 A. S. S. Wilson, M. S. Hill, M. F. Mahon, C. Dinoi and L. Maron, *Science*, 2017, **358**, 1168–1171.
26 B. Maitland, M. Wiesinger, J. Langer, G. Ballmann, J. Pahl, H. Elsen, C. Farber and S. Harder, *Angew. Chem., Int. Ed.*, 2017, **56**, 11880–11884.
27 J. Yin, Y. Hu and J. Yoon, *Chem. Soc. Rev.*, 2015, **44**, 4619–4644.
28 M. J. Berridge, M. D. Bootman and H. L. Roderick, *Nat. Rev. Mol. Cell Biol.*, 2003, **4**, 517–529.
29 P. J. Marie, P. Ammann, G. Boivin and C. Rey, *Calcif. Tissue Int.*, 2001, **69**, 121–129.
30 R.-M. Han, Y.-X. Tian, E. M. Becker, M. L. Andersen and L. H. Skibsted, *J. Agric. Food Chem.*, 2007, **55**, 2384–2391.
31 R.-M. Han, C.-H. Chen, Y.-X. Tian, J.-P. Zhang and L. H. Skibsted, *J. Phys. Chem. A*, 2010, **114**, 126–132.
32 V. Butković, L. Klasinc and W. Bors, *J. Agric. Food Chem.*, 2004, **52**, 2816–2820.
33 B. P. Pritchard, D. Altarawy, B. Didier, T. D. Gibson and T. L. Windus, *J. Chem. Inf. Model.*, 2019, **59**, 4814–4820.
34 J. E. Bartmess, *J. Phys. Chem.*, 1994, **98**, 6420–6424.
35 M. J. Stowell, Handbook of chemistry and Physics 50th edn, *Phys. Bull.*, 1970, **21**, 460.
36 G.-X. Xu, *Substance Structure*, Higher Education Press, Beijing, 2nd edn, 1991.
37 R. A. Dar, G. A. Naikoo, I. U. Hassan and A. M. H. Shaikh, *Anal. Chem. Res.*, 2016, **7**, 1–8.
38 Y. Oztekin, Z. Yazicigil, A. Ramanaviciene and A. Ramanavicius, *Sens. Actuators, B*, 2011, **152**, 37–48.
39 Y.-J. Shang, Y.-P. Qian, X.-D. Liu, F. Dai, X.-L. Shang, W.-Q. Jia, Q. Liu, J.-G. Fang and B. Zhou, *J. Org. Chem.*, 2009, **74**, 5025–5031.

40 L.-L. Song, R. Liang, D.-D. Li, Y.-D. Xing, R.-M. Han, J.-P. Zhang and L. H. Skibsted, *J. Agric. Food Chem.*, 2011, **59**, 12643–12651.
41 H. Cheng, R.-M. Han, J.-P. Zhang and L. H. Skibsted, *J. Agric. Food Chem.*, 2014, **62**, 942–949.
42 S. B. Bukhari, S. Memon, M. Mahroof-Tahir and M. I. Bhanger, *Spectrochim. Acta, Part A*, 2009, **71**, 1901–1906.
43 G. Dehghan and Z. Khoshkam, *Food Chem.*, 2012, **131**, 422–426.